INTERNATIONAL JOURNAL FOR NUMERICAL METHODS IN FLUIDS
Int. J. Numer. Meth. Fluids 2009; **60**:919–936
Published online 29 September 2008 in Wiley InterScience (www.interscience.wiley.com). DOI: 10.1002/fld.1925

Investigation of incompressible flow within $\frac{1}{2}$ circular cavity using lattice Boltzmann method

Lixia Ding, Weiping Shi*, †, Hongwen Luo and Haicheng Zheng

College of Mathematics, Jilin University, Changchun 130012, China

SUMMARY

A wall-driven incompressible viscous flow in a $\frac{1}{2}$ circular cavity is simulated, based on the lattice Boltzmann method (LBM). The treatment of curved boundary with second-order accuracy is used. The force evaluation is based on the momentum-exchange method. The streamlines and vorticity contours and the velocity component along the central line of a semi-circular cavity are obtained for different Reynolds numbers. The numerical results show that the LBM can capture the formation of primary, secondary and tertiary vortices exactly as the Reynolds number increases and has a great agreement with those of current literatures. Copyright © 2008 John Wiley & Sons, Ltd.

Received 10 April 2008; Revised 16 August 2008; Accepted 19 August 2008

KEY WORDS: lattice Boltzmann method; $\frac{1}{2}$ circular cavity flow; curved boundary; the momentum-exchange method; incompressible flow; vortex center

1. INTRODUCTION

The lattice Boltzmann method (LBM) has recently become an alternative method for computational fluid dynamics and has achieved great success in simulating a wide variety of physical systems in the past decades [1–8], such as multi-phase flow, suspension flow and flow in the porous media, which are quite difficult to simulate by conventional methods. This method can be either regarded as an extension of the lattice gas automation [9] or as a special discrete form of the Boltzmann equation for kinetic theory. Unlike conventional methods, which are based on macroscopic continuity equations to determine macroscopic fluid dynamics, LBM is based on the microscopic dynamics of fluid. Basically, it has two processes: streaming and collision. The LBM has demonstrated a significant potential and broad applicability with many computational advantages including easy handling of complex boundary conditions, efficient hydrodynamics simulations, the parallel of

*Correspondence to: Weiping Shi, College of Mathematics, Jilin University, Changchun 130012, China.
†E-mail: shiwp@jlu.edu.cn

Contract/grant sponsor: The 985 project of Jilin University; contract/grant number: 985

algorithms and the simplicity of programming. In the foreseeable future, the LBM method is likely to play a significant role in the numerical prediction of flows. An introduction to the LBM theory, methodology and the current status may be obtained from References [10–12].

Numerical methods for two-dimensional steady incompressible Navier–Stokes equations are often tested for code validation, such as the lid-driven cavity flow, a very well-known benchmark problem [13–15]. Owing to the simplicity of the cavity geometry, applying a numerical method on this flow problem in terms of coding is quite easy and straightforward. It is possible to find different numerical approaches that have been applied to the driven cavity flow problem [16–24], such as finite differences, finite elements, spectral analysis, lattice Boltzmann, multi-grid, etc. Fluid flows in a circular cavity have been less studied than those in a square cavity, even though the two flow patterns have geometric similarities, on account of the complex boundary conditions. For example, Glowinski *et al.* [21] employed an operator-splitting/finite elements method to handle fluid flow in a semi-circular cavity and captured the formation of primary, secondary and tertiary vortices and identified a Hopf bifurcation phenomenon around $Re=6600$. Erturk *et al.* [17] presented numerical solutions of the two-dimensional steady incompressible driven cavity flow for $Re<21\,000$ by using the stream function and vorticity formation of the Navier–Stokes equations. Hou *et al.* [13] simulated the cavity flow by LBM and presented solutions for $Re=7500$. They made extensive comparison of LBM results with Navier–Stokes solution results of Ghia *et al.* [16]. Nishida and Satofuka [18] presented a new higher-order method for the simulation of the driven cavity flow.

In this article, our main goal is to investigate the capability of LBM for handling incompressible viscous flow accurately at large Reynolds number in regions with corners and curved boundaries and capturing bifurcation phenomenon as the Reynolds number increases. A wall-driven flow in a two-dimensional semi-circular cavity problem is investigated.

In the following section, the mathematical formulation of the lattice Boltzmann model is described. In Section 3, a wall-driven flow in two-dimensional semi-circular domain is simulated numerically, and Section 4 gives concluding remarks.

2. MATHEMATICAL FORMULATION

2.1. Background of the lattice Boltzmann equation

The most widely used lattice Boltzmann equation is a discretized version of the model Boltzmann equation with a single relaxation time factor due to Bhatnagar *et al.* [25]. A D2Q9 scheme is adopted in this work, where D refers to space dimensions and Q to the number of different velocity at a computational node. Here, each node comprises eight moving particles and a rest particle (see Figure 1). A discrete velocity model of the Boltzmann equation discreted in space $\mathbf{x}$ and time t is given by

$$f_\alpha(\mathbf{x}+\mathbf{e}_\alpha\delta_t, t+\delta_t) - f_\alpha(\mathbf{x}, t) = -\frac{1}{\tau}[f_\alpha(\mathbf{x}, t) - f_\alpha^{(\mathrm{eq})}(\mathbf{x}, t)] \tag{1}$$

where $\mathbf{e}_\alpha(\alpha=0, 1, \ldots, 8)$ is a discrete velocity vector,

$$[\mathbf{e}_0, \mathbf{e}_1, \mathbf{e}_2, \mathbf{e}_3, \mathbf{e}_4, \mathbf{e}_5, \mathbf{e}_6, \mathbf{e}_7, \mathbf{e}_8] = \begin{bmatrix} 0 & 1 & 1 & 0 & -1 & -1 & -1 & 0 & 1 \\ 0 & 0 & 1 & 1 & 1 & 0 & -1 & -1 & -1 \end{bmatrix} c, \quad f_\alpha(\mathbf{x}, t)$$

DOI: 10.1002/fld

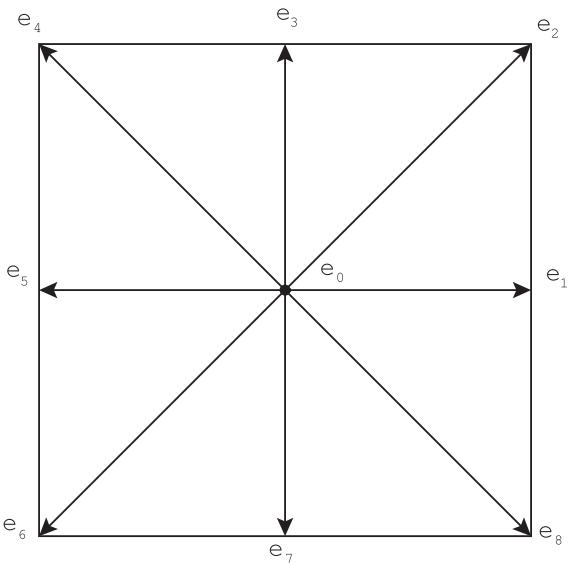

Figure 1. Discrete velocity set of two-dimensional nine-velocity (D2Q9) model.

is particle distribution function, also named population, and $f_\alpha^{(\mathrm{eq})}(\mathbf{x},t)$ is the equilibrium distribution function of the αth discrete velocity, respectively, δ_t is time step and τ is the dimensionless relaxation time, which is related to the kinetic viscosity $v=\frac{1}{3}(\tau-\frac{1}{2})$.

The equilibrium distribution function $f_\alpha^{(\mathrm{eq})}(\mathbf{x},t)$ in Equation (1) is obtained by expanding the Maxwell–Boltzmann distribution function in Taylor series of $\mathbf{u}$ up to second order [5] and can be expressed in general as

$$f_\alpha^{(\mathrm{eq})}(\mathbf{x},t)=\omega_\alpha\rho\left[1+\frac{3}{c^2}(\mathbf{e}_\alpha\cdot\mathbf{u})+\frac{9}{2c^4}(\mathbf{e}_\alpha\cdot\mathbf{u})^2-\frac{3}{2c^2}\mathbf{u}^2\right] \tag{2}$$

where $c\equiv\delta_x/\delta_t$, δ_x is the lattice length of the underlying lattice space; in this work the lattice length δ_x and time step δ_t are set to be a unit, then c is a unit velocity, the coefficient ω_α depends on the discrete velocity ($\omega_\alpha=\frac{4}{9}$ for $\alpha=0$; $\omega_\alpha=\frac{1}{9}$ for $\alpha=1$–4; $\omega_\alpha=\frac{1}{36}$ for $\alpha=5$–8), the speed of sound is $c_\mathrm{s}=c/\sqrt{3}$. The lattice Boltzmann models should describe the dynamics of macroscopic variables. The macroscopic variables $\mathbf{u}$, ρ are some linear combinations of the distribution function at the same point. The macroscopic variables are invariants of collisions

$$\rho=\sum_\alpha f_\alpha,\quad \rho\mathbf{u}=\sum_\alpha \mathbf{e}_\alpha f_\alpha \tag{3}$$

The single-particle distribution function $f_\alpha(\mathbf{x},t)$ is evolved by advection and collision on a fixed computational lattice. During the collision step, the particles readjust their states while the overall mass and momentum at the computational node are conserved. In the subsequent step, that is advection, the particles move to the nearest neighbors along their respective velocity direction.

DOI: 10.1002/fld

That is,

$$\text{Collision: } \tilde{f}_\alpha(\mathbf{x},t)=f_\alpha(\mathbf{x},t)-\frac{1}{\tau}[f_\alpha(\mathbf{x},t)-f_\alpha^{(\mathrm{eq})}(\mathbf{x},t)] \tag{4a}$$

$$\text{Advection: } f_\alpha(\mathbf{x}+\mathbf{e}_\alpha\delta_t,t+\delta_t)=\tilde{f}_\alpha(\mathbf{x},t) \tag{4b}$$

where $\tilde{f}_\alpha(\mathbf{x},t)$ is an intermediate particle distribution function. The computational process is explicit and parallel naturally. The collision step is completely local and the advection step is uniform and requires little computational efforts.

The Navier–Stokes equations are recovered in near incompressible limit (i.e. the Mach number $Ma=|\mathbf{u}|/c_\mathrm{s}\leqslant 0.3$) by the Chapman–Enskog expanding

$$\begin{aligned}\nabla\cdot\mathbf{u}&=0\\ \mathbf{u}_t+(\mathbf{u}\cdot\nabla)\mathbf{u}&=-\nabla p+\nu\Delta\mathbf{u}\end{aligned} \tag{5}$$

where p is the fluid pressure, which is given by $p=c_\mathrm{s}^2\rho$, with $c_\mathrm{s}=1/\sqrt{3}$ being the dimensionless speed of sound.

2.2. *The curved boundary treatment*

Consider a part of an arbitrary curved boundary, as shown in Figure 2, where $\mathbf{x}_w$ denotes the intersections of the boundary with various lattice-to-lattice links, $\mathbf{x}_\mathrm{f}$ denotes the fluid node near the boundary and $\mathbf{x}_b$ denotes the solid node near the boundary. The fraction of an intersected link in the fluid region, Δ, is defined by $\Delta=\|x_\mathrm{f}-x_w\|/\|x_\mathrm{f}-x_b\|$. Obviously, $0\leqslant\Delta\leqslant 1$ and the horizontal or vertical distance between $\mathbf{x}_b$ and $\mathbf{x}_w$ is $\Delta\delta_x$ on the square lattice.

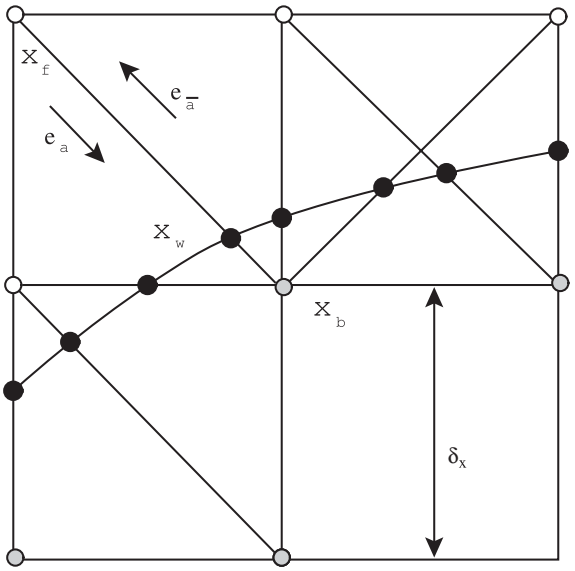

Figure 2. Layout of the regularly spaced lattices and curved wall boundary.

DOI: 10.1002/fld

Generally, the bounce-back boundary condition has been used to deal with a solid boundary in order to approximate the no-slip boundary condition. However, it is well understood that this bounce-back boundary condition satisfies the no-slip boundary condition with a second-order accuracy at the location one-half lattice spacing ($\Delta=\frac{1}{2}$) outside of a boundary node where the bounce-back collision takes place; and this is only true with simple boundaries of straight lines parallel to the lattice grid [26]. For a curved boundary, simply placing the boundary halfway between two nodes will alter the geometry on the grid level and decrease the accuracy of the flow field and the force on the body.

Because the bounce-back boundary condition plays an important role in lattice Boltzmann simulations, substantial works have been done to improve the accuracy. A second-order accurate boundary condition for curved geometry was developed in conjunction with the use of a Cartesian grid in order to retain the advantages of the LBM. An interpolation scheme is employed only at the boundaries to obtain $\tilde{f}_\alpha(x_i,t)$. The detailed assessment on the impact of the boundary condition on the accuracy of the flow field has been given in Reference [27]. Substantial evidence shows that the bounce-back boundary conditions combined with interpolations, and including the one-half grid spacing correction at boundaries, are in fact second-order accurate and capable of handling curved boundaries. Suppose the particle momentum moving from $\mathbf{x}_\mathrm{f}$ to $\mathbf{x}_b$ is $\mathbf{e}_\alpha$ and the reversed one from $\mathbf{x}_b$ to $\mathbf{x}_\mathrm{f}$ is $\mathbf{e}_{\overline{\alpha}}=-\mathbf{e}_\alpha$, after the collision step, $\tilde{f}_\alpha(\mathbf{x},t)$ on the fluid side is known, but not on the solid side. Here, we shall use $\mathbf{e}_{\overline{\alpha}}$ and $f_{\overline{\alpha}}$ to denote the velocity and the distribution function coming from a solid node to a fluid node, and $f_{\overline{\alpha}}$ is the unknown variable. To finish the advection step

$$f_{\overline{\alpha}}(\mathbf{x}_b+\mathbf{e}_{\overline{\alpha}}\delta_t,t+\delta_t)=\tilde{f}_{\overline{\alpha}}(\mathbf{x}_b,t)$$

where Filippova and Hänel [28] proposed the linear interpolation

$$f_{\overline{\alpha}}(\mathbf{x}_b,t)=(1-\chi)\tilde{f}_\alpha(\mathbf{x}_\mathrm{f},t)+\chi f_\alpha^{(*)}(\mathbf{x}_\mathrm{f},t)+2w_\alpha\rho\frac{3}{c^2}\mathbf{e}_{\overline{\alpha}}\cdot\mathbf{u}_\mathrm{w} \tag{6}$$

where $\mathbf{u}_\mathrm{w}$ is the velocity at the wall and χ is the weighing factor that controls the linear interpolation or extrapolation between $\tilde{f}_\alpha(\mathbf{x}_\mathrm{f},t)$ and $f_\alpha^*(\mathbf{x}_b,t)$, a fictitious equilibrium distribution function given by

$$\begin{aligned} f_\alpha^{(*)}(\mathbf{x}_b,t) &= w_\alpha\rho\left[1+\frac{3}{c^2}(\mathbf{e}_\alpha\cdot\mathbf{u}_{bf})+\frac{9}{2c^4}(\mathbf{e}_\alpha\cdot\mathbf{u}_f)^2-\frac{3}{2c^2}\mathbf{u}_f^2\right] \\ &= f_\alpha^{(\mathrm{eq})}(\mathbf{x}_\mathrm{f},t)+w_\alpha\rho\frac{3}{c^2}\mathbf{e}_\alpha\cdot(\mathbf{u}_{bf}-\mathbf{u}_f) \end{aligned} \tag{7}$$

Here, $\mathbf{u}_{bf}$ and χ are given by

$$\mathbf{u}_{bf}=\mathbf{u}_f(x_\mathrm{f}+\mathbf{e}_{\overline{\alpha}}\delta_t,t),\quad \chi=\frac{2\Delta-1}{\tau-2},\quad 0\leqslant\Delta\leqslant 0.5$$

$$\mathbf{u}_{bf}=\frac{2\Delta-3}{2\Delta}\mathbf{u}_f+\frac{3}{2\Delta}\mathbf{u}_\mathrm{w},\quad \chi=\frac{2\Delta-1}{\tau+0.5},\quad 0.5\leqslant\Delta<1$$

DOI: 10.1002/fld

By applying Chapman–Enskog expansion for the distribution function at the boundary

$$\tilde{f}_{\overline{\alpha}}(\mathbf{x}_b, t) = \tilde{f}_{\alpha}(\mathbf{x}_\mathrm{f}, t) - \chi[\tilde{f}_{\alpha}(\mathbf{x}_\mathrm{f}, t) - f_{\alpha}^{(\mathrm{eq})}(\mathbf{x}_\mathrm{f}, t)] + \omega_{\alpha}\rho(\mathbf{x}_\mathrm{f}, t)\frac{3}{c^2}\mathbf{e}_{\alpha}\cdot[\chi(\mathbf{u}_{bf} - \mathbf{u}_f) - 2\mathbf{u}_\mathrm{w}] \tag{8}$$

the treatment of boundary condition can lead to a second-order accurate no-slip boundary condition [29].

2.3. The force evaluation based on the momentum-exchange method

One important issue is the accurate determination of the fluid dynamic force involving curved boundaries in the LBM simulation. In addition to an estimate of shear stress, τ_{21}, via the partial derivative of the mean velocity profile, that is $\tau_{21} = \mu \mathrm{d}u/\mathrm{d}y$, the lattice Boltzmann approach provides an alternative way of computing the viscous shear stress [27]

$$\tau_{21} = \left(1 - \frac{1}{2\tau}\right)\sum_i f_i^{\mathrm{neq}} e_{ix} e_{iy}$$

where $f_i^{\mathrm{neq}} = f_i - f_i^{\mathrm{eq}}$ is the nonequilibrium distribution function, e_{ix} and e_{iy} are the xth and yth Cartesian component of the discrete velocity e_i, respectively. An advantage of this approach compared with the partial derivative is that it is local and thus provides an accurate measure of the immediate vicinity of the wall.

Several force evaluation schemes, including momentum-exchange and integration of surface stress [27], have been used. In this work, the momentum-exchange method will be employed.

An array $w(i, j)$ is first introduced

$$w(i, j) = \begin{cases} 0 & \text{for fluid nodes} \\ 1 & \text{for solid nodes} \end{cases}$$

For a given boundary node $\mathbf{x}_\mathrm{b}$ inside the solid region, the momentum-exchange with all possible neighboring fluid nodes over a time step is

$$\sum_{\alpha \neq 0} \mathbf{e}_{\alpha}[\tilde{f}_{\alpha}(\mathbf{x}_\mathrm{b}, t) + \tilde{f}_{\overline{\alpha}}(\mathbf{x}_\mathrm{b} + \mathbf{e}_{\overline{\alpha}}\delta_t, t)][1 - w(\mathbf{x}_\mathrm{b} + \mathbf{e}_{\overline{\alpha}}\delta_t)]$$

Simply summing the contribution over all boundary nodes $\mathbf{x}_\mathrm{b}$ belonging to the body, the total force acted by the solid body on the fluid is obtained as

$$F = \sum_{all\ \mathbf{x}_\mathrm{b}} \sum_{\alpha \neq 0} \mathbf{e}_{\alpha}[\tilde{f}_{\alpha}(\mathbf{x}_\mathrm{b}, t) + \tilde{f}_{\overline{\alpha}}(\mathbf{x}_\mathrm{b} + \mathbf{e}_{\overline{\alpha}}\delta_t, t)][1 - w(\mathbf{x}_\mathrm{b} + \mathbf{e}_{\overline{\alpha}}\delta_t)] \tag{9}$$

The force F is evaluated after the collision step is carried out. The effect of Δ is implicit taken into account in the determination of $\tilde{f}_{\overline{\alpha}}(\mathbf{x}_\mathrm{b}, t + \delta_t)$.

DOI: 10.1002/fld

3. NUMERICAL SIMULATION

3.1. Problem description and boundary conditions

An incompressible viscous fluid fills a $\frac{1}{2}$ circular cavity where the straight part of the boundary is translating with an assigned velocity and the curvilinear part maintains motionless, as shown in Figure 3. The domain occupied by the fluid is the two-dimensional region of space.

In the present simulation, the computation domain with $512\delta_x \times 256\delta_x$ lattice is selected, the streaming velocity U is given. The Reynolds number is defined as $Re = UD/\nu$, where D is the characteristic length of the domain, U is the characteristic velocity of the fluid, ν is the kinetic viscosity of the fluid. Here, we have taken U equal to the norm of the sliding velocity of the upper wall and D equal to the diameter of the cavity. The dimensionless drag coefficient $C_D = F_D/(0.5\rho U^2 D)$, where F_D is the drag force acted on solid body.

3.2. Effects of the Reynolds number

The effects of the Reynolds number on the cavity flow are examined. The fluid flow is researched for the Reynolds number in the sequence $500, 1000, 2000, 3000, 5000, 6600$. When the Reynolds number is large enough, the solution does not reach a steady state anymore but shows an oscillatory behavior. The simulation is terminated when the following criterion based on the relative L_2-norm error in the fluid region Ω is satisfied

$$E_2 = \sqrt{\frac{\sum_{x_i \in \Omega} \|\mathbf{u}(x_i, t+1) - \mathbf{u}(x_i, t)\|^2}{\sum_{x_i \in \Omega} \|\mathbf{u}(x_i, t+1)\|^2}} \leqslant \varepsilon \tag{10}$$

In this work, $\varepsilon = 10^{-6}$ was chosen.

Steady states were reached for the Reynolds number up to 6600, streamlines, vorticity contours of the steady states for $Re = 500, 1000, 2000, 3000, 5000, 6600$ are reported in Figures 4–9. The stream function, which is not a primary variable in the LBM simulation, is obtained from the velocity data by integration. That is $u = \psi_y, v = -\psi_x$, and vorticity function can be obtained by the following formulation $w = v_x - u_y$. When the Reynolds number is small, the final steady state

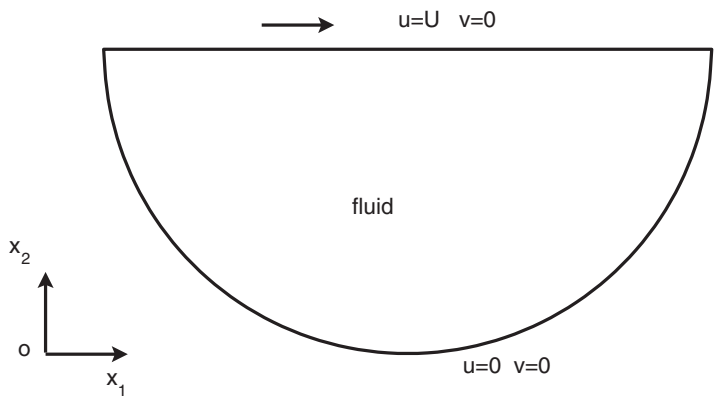

Figure 3. Wall-driven flow in a semi-circular cavity.

DOI: 10.1002/fld

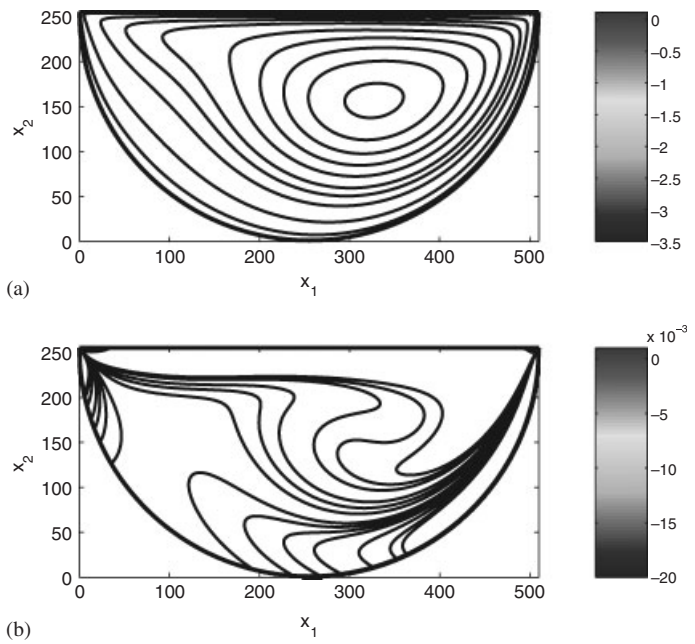

Figure 4. Streamlines and vorticity contours for $Re = 500$: (a) streamlines and (b) vorticity contours.

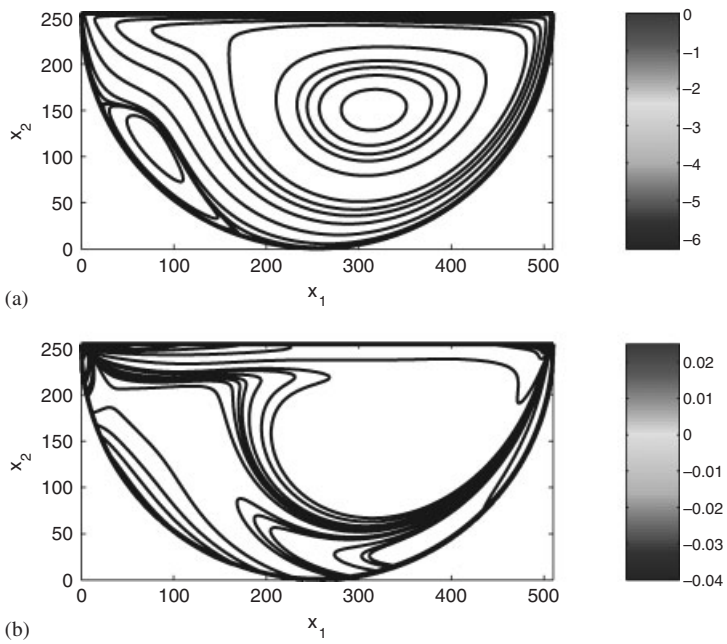

Figure 5. Streamlines and vorticity contours for $Re = 1000$: (a) streamlines and (b) vorticity contours.

DOI: 10.1002/fld

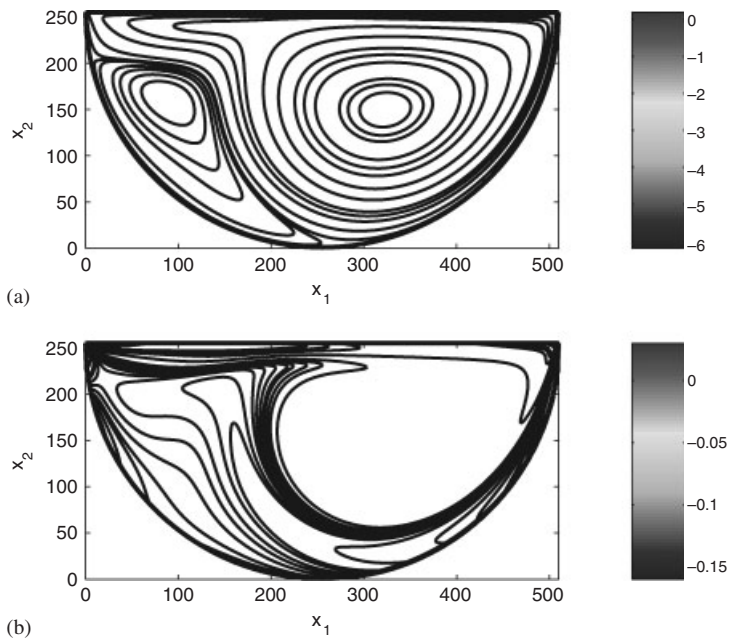

Figure 6. Streamlines and vorticity contours for $Re = 2000$: (a) streamlines and (b) vorticity contours.

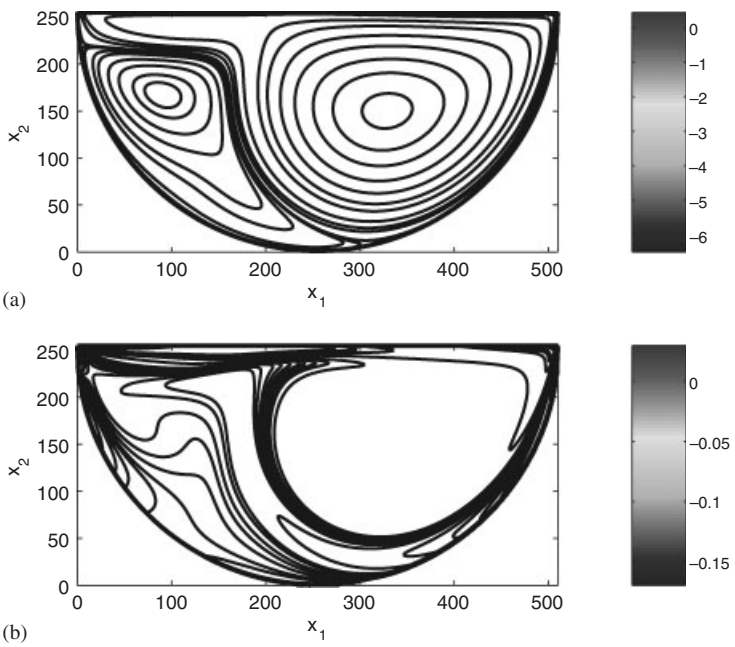

Figure 7. Streamlines and vorticity contours for $Re = 3000$: (a) streamlines and (b) vorticity contours.

DOI: 10.1002/fld

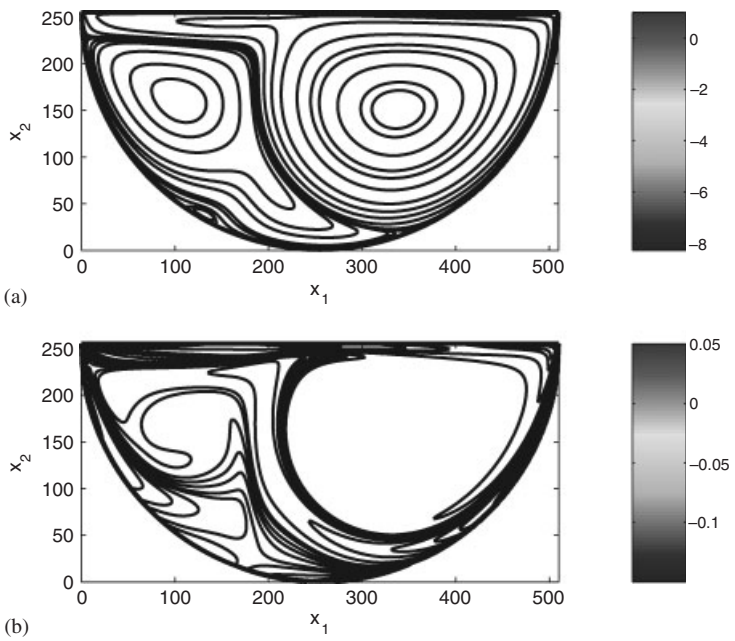

Figure 8. Streamlines and vorticity contours for $Re = 5000$: (a) streamlines and (b) vorticity contours.

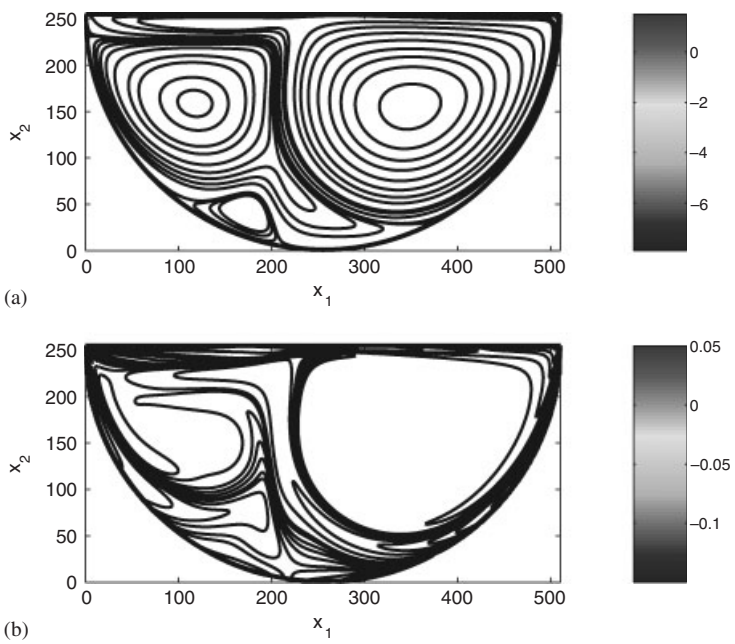

Figure 9. Streamlines and vorticity contours for $Re = 6600$: (a) streamlines and (b) vorticity contours.

DOI: 10.1002/fld

consists of one vortex only and no separation occurs. As the Reynolds number increases, separation occurs and the size and shape of the separated region changes and first a secondary vortex and then a tertiary vortex arises. As we can see in Figures 4–9. Figures 10–15 show the results of Reference [21] at $Re = 500, 1000, 2000, 3000, 5000, 6600$, respectively. The present result agrees well with Reference [21].

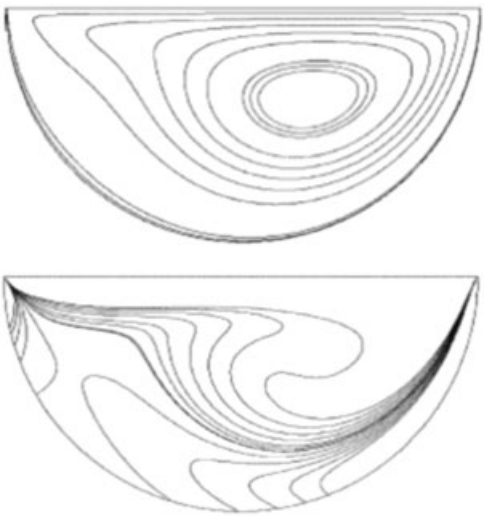

Figure 10. Streamlines and vorticity contours for $Re = 500$ in Reference [21]. The top one is streamlines and the bottom one is vorticity contours.

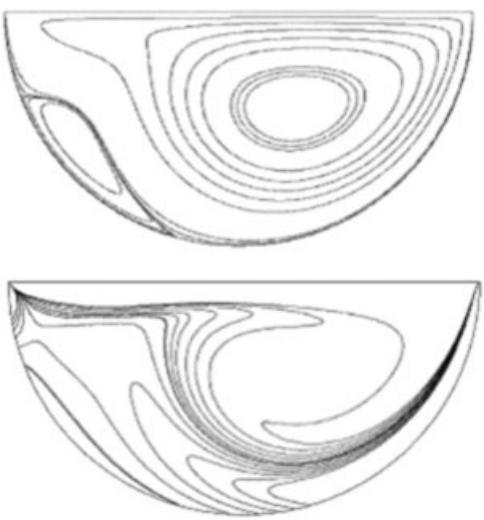

Figure 11. Streamlines and vorticity contours for $Re = 1000$ in Reference [21]. The top one is streamlines and the bottom one is vorticity contours.

DOI: 10.1002/fld

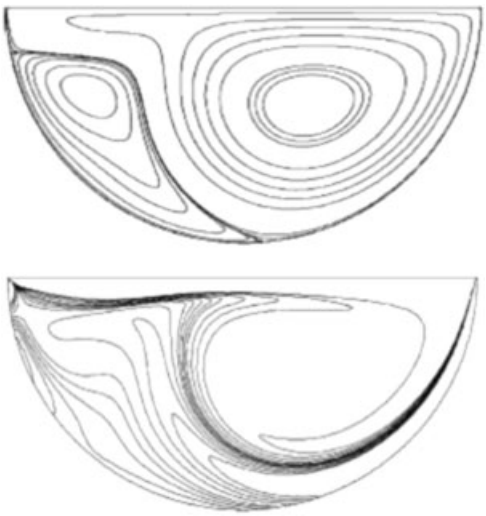

Figure 12. Streamlines and vorticity contours for $Re=2000$ in Reference [21]. The top one is streamlines and the bottom one is vorticity contours.

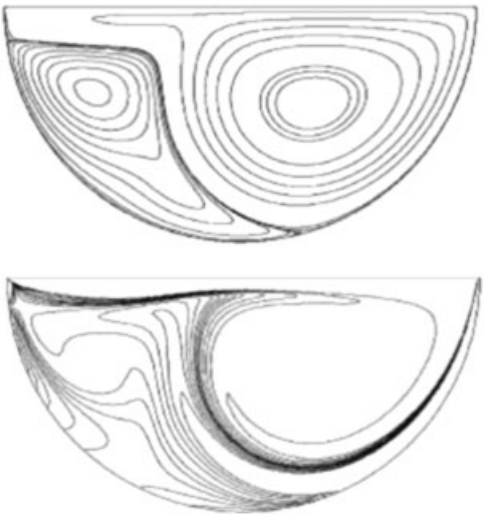

Figure 13. Streamlines and vorticity contours for $Re=3000$ in Reference [21]. The top one is streamlines and the bottom one is vorticity contours.

The fluid motion generated in this cavity is an example of closed streamline problems that are of theoretical importance because they are part of a broader field of steady, separated flows. Unlike in the square cavity, a major vortex occupies the central part of the domain while minor vortices appear at the lower corners and the top-left [13]. In the case of $\frac{1}{2}$ circular cavity, the

DOI: 10.1002/fld

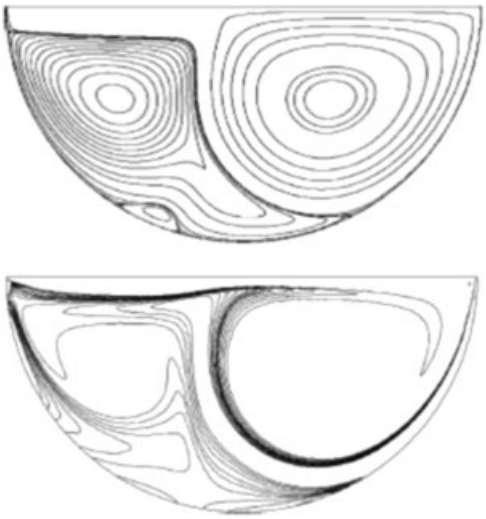

Figure 14. Streamlines and vorticity contours for $Re=5000$ in Reference [21]. The top one is streamlines and the bottom one is vorticity contours.

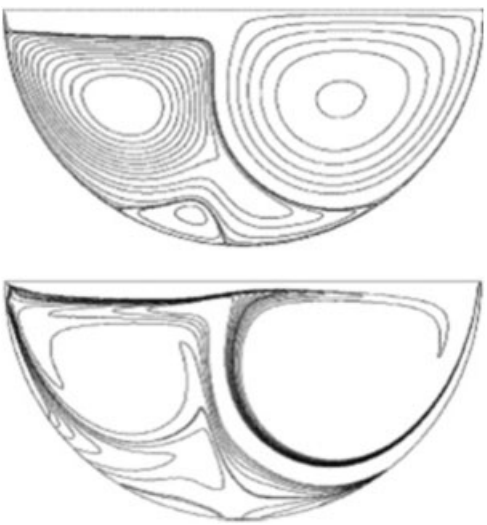

Figure 15. Streamlines and vorticity contours for $Re=6600$ in Reference [21]. The top one is streamlines and the bottom one is vorticity contours.

vortices develop at the bottom and as the Reynolds number increases, they grow pushing the main vortex to the right part of the cavity. Vortex centers are characterized as the local extremum of the stream function. Actually, this phenomenon is tracked by the point where the minimum value of the stream function ψ is attained.

DOI: 10.1002/fld

In Table I, we have summarized the minimum value of ψ and its location at various Reynolds numbers and given the result of center of primary vortex in Reference [21].

The effects of the Reynolds number on the velocity distribution are also examined. The u-velocity component along the line $x_1 = \frac{1}{2}$ and v-velocity component along the line $x_2 = \frac{1}{4}$ are presented and

Table I. Properties of vortices, minimum stream function value and location of center of vortices.

Reynolds number	Minimum stream function Ψ	Center of primary vortex	Center of secondary vortex	Center of tertiary vortex	Center of primary vortex in Reference [21]
500	−0.0099	(0.6423, 0.3099)	—	—	—
1000	−0.0187	(0.6221, 0.2983)	(0.1566, 0.2230)	—	(0.6156, 0.2971)
2000	−0.0178	(0.6309, 0.2955)	(0.1750, 0.3156)	—	(0.6329, 0.2958)
3000	−0.0184	(0.6468, 0.2971)	(0.1795, 0.3281)	—	(0.6548, 0.2969)
5000	−0.0550	(0.6715, 0.3027)	(0.2124, 0.3196)	(0.2752, 0.0752)	(0.6809, 0.3012)
6600	−0.0216	(0.6804, 0.3112)	(0.2327, 0.3156)	(0.3405, 0.0841)	(0.7006, 0.3106)

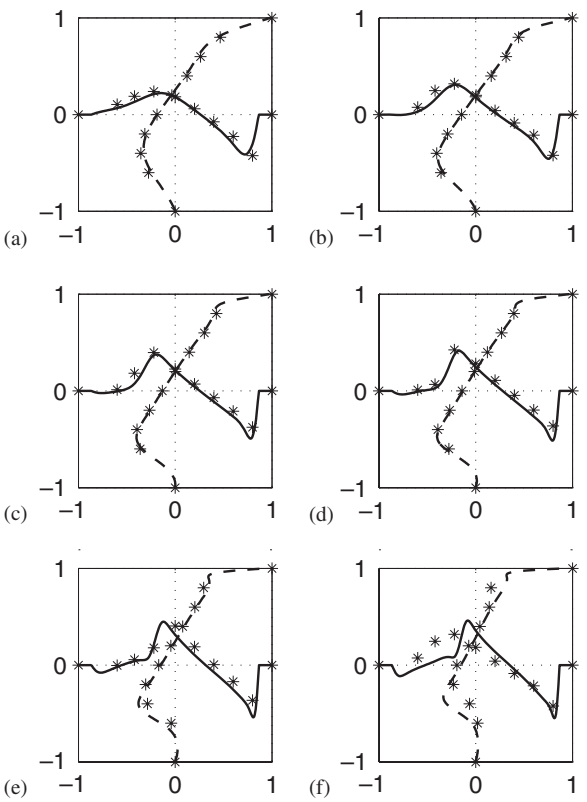

Figure 16. The comparison of the velocity profile for different Reynolds numbers. The dashed line represents the u-velocity component along the line $x_1 = \frac{1}{2}$, while the solid line represents the v-velocity component along the line $x_2 = \frac{1}{4}$, the asterisk $(*)$ represents the result of Reference [21], respectively: (a) $Re = 500$; (b) $Re = 1000$; (c) $Re = 2000$; (d) $Re = 3000$; (e) $Re = 5000$; and (f) $Re = 6600$.

DOI: 10.1002/fld

the comparison of the velocity profile for present result with that of Reference [21] are shown in Figure 16.

Some selection values corresponding to the profiles are listed in Tables II and III.

It is shown that our results have a great agreement with those in the current literatures and validate LBM in dealing with the case.

Table II. Tabulated u-velocity component along the line $x_1 = \frac{1}{2}$ at various Reynolds numbers.

x_2	$Re=500$	$Re=1000$	$Re=2000$	$Re=3000$	$Re=5000$	$Re=6600$
0.0000	0.0000	0.0000	0.0000	0.0000	0.0000	0.0000
0.0275	−0.0571	−0.0613	−0.0222	0.0054	0.0245	0.0202
0.0569	−0.1322	−0.1701	−0.1289	−0.0745	0.0093	0.0209
0.0863	−0.2121	−0.2906	−0.2849	−0.2415	−0.0794	−0.0098
0.1157	−0.2807	−0.3728	−0.3891	−0.3808	−0.2603	−0.1153
0.1451	−0.3208	−0.3869	−0.3864	−0.3862	−0.3773	−0.2762
0.1745	−0.3228	−0.3430	−0.3219	−0.3178	−0.3416	−0.3160
0.2039	−0.2880	−0.2702	−0.2454	−0.2422	−0.2621	−0.2539
0.2333	−0.2259	−0.1888	−0.1704	−0.1701	−0.1863	−0.1824
0.2628	−0.1477	−0.1057	−0.0958	−0.0988	−0.1141	−0.1174
0.2922	−0.0619	−0.0211	−0.0198	−0.0264	−0.0434	−0.0567
0.3216	0.0254	0.0661	0.0588	0.0478	0.0267	0.0016
0.3510	0.1094	0.1556	0.1408	0.1246	0.0971	0.0591
0.3804	0.1862	0.2437	0.2273	0.2059	0.1696	0.1181
0.4098	0.2606	0.3211	0.3143	0.2931	0.2474	0.1828
0.4392	0.3712	0.3842	0.3830	0.3734	0.3244	0.2563
0.4686	0.6019	0.5314	0.4350	0.4094	0.3512	0.3098
0.5000	0.9826	0.9810	0.9729	0.9661	0.9406	0.8754

Table III. Tabulated v-velocity component along the line $x_2 = \frac{1}{4}$ at various Reynolds numbers.

x_1	$Re=500$	$Re=1000$	$Re=2000$	$Re=3000$	$Re=5000$	$Re=6600$
0.0000	0.0000	0.0000	0.0000	0.0000	0.0000	0.0000
0.1157	0.0292	−0.0041	−0.0226	−0.0364	−0.0782	−0.1120
0.1745	0.0547	0.0137	−0.0129	−0.0192	−0.0399	−0.0532
0.2333	0.0872	0.0640	0.0095	0.0039	0.0064	−0.0046
0.2922	0.1335	0.1607	0.0801	0.0305	0.0423	0.0433
0.3510	0.1857	0.2727	0.2666	0.1962	0.0591	0.0836
0.4098	0.2194	0.3033	0.3757	0.4126	0.3498	0.1669
0.4686	0.2085	0.2307	0.2762	0.3139	0.3939	0.4493
0.5275	0.1504	0.1301	0.1638	0.1937	0.2523	0.2884
0.5863	0.0665	0.0387	0.0653	0.0884	0.1313	0.1644
0.6451	−0.0229	−0.0452	−0.0279	−0.0106	0.0226	0.0555
0.7039	−0.1146	−0.1258	−0.1183	−0.1063	−0.0795	−0.0514
0.7627	−0.2235	−0.2101	−0.2080	−0.2026	−0.1828	−0.1641
0.8216	−0.3586	−0.3339	−0.3033	−0.3021	−0.2966	−0.2878
0.8804	−0.3879	−0.4555	−0.4809	−0.4704	−0.4475	−0.4292
1.0000	0.0000	0.0000	0.0000	0.0000	0.0000	0.0000

DOI: 10.1002/fld

Further, the drag coefficient decreases as Re increases, as found in other laminar flow configurations. This can be seen by introducing the dimensionless quantities

$$u' = \frac{u}{U}, \quad x' = \frac{x_1}{D}, \quad y' = \frac{x_2}{12D} \tag{11}$$

The stress on the wall is given by Newton's formula

$$\tau_{21} = \mu \frac{\partial u}{\partial x_2} \tag{12}$$

where u is the x_1 component of velocity and μ is the kinetic viscosity. The drag force on this surface, F_D, is defined in Equation (9) and computed also as

$$F_D = \int_0^D \tau_{21}\, dx_1 = \int_0^1 \mu \frac{U \partial u'}{1/2D \partial y'} D\, dx' = \int_0^1 2\mu U \frac{\partial u'}{\partial y'}\, dx' \tag{13}$$

The drag coefficient can then be expressed as

$$C_D = \frac{2F_D}{\rho U^2 D} = \frac{4}{Re} \int_0^1 \frac{\partial u'}{\partial y'}\, dx' \tag{14}$$

Figure 17 shows the comparison of the dimensionless drag coefficient for $\frac{1}{2}$ circular cavity with that of a plane for different Reynolds numbers. The present result is gradually close to that of a plane as the Reynolds number increases. The drag coefficient of a plane $C_D^{\text{plane}} = 1.328/\sqrt{Re}$. It suggests that our result agrees well with the theoretical value.

The evolution of the L_2-norm of the velocity in the neighborhood of the critical point can be seen from Figure 18. For $Re = 6600$, a steady state is reached: the L_2-norm of the velocity gets flat.

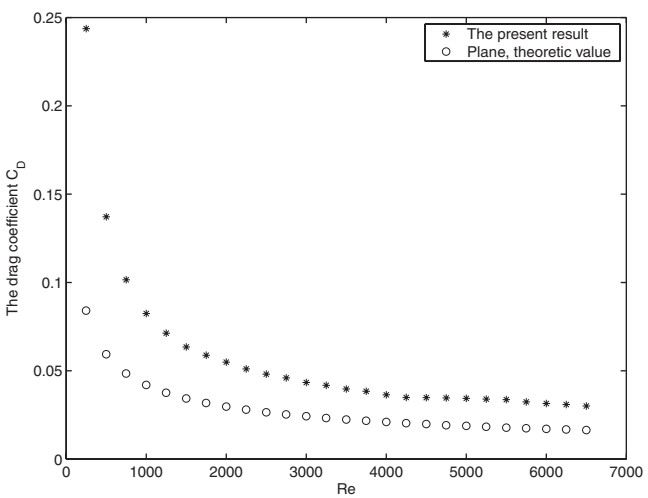

Figure 17. Comparison of the drag coefficient for the present result with that of a plane (theoretic value) for different Reynolds numbers.

DOI: 10.1002/fld

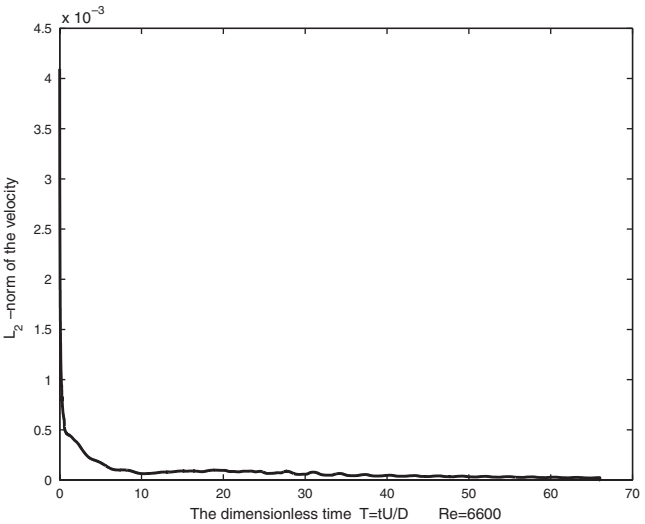

Figure 18. Evolution of the L_2-norm of the velocity for $Re = 6600$.

4. CONCLUDING REMARKS

A wall-driven flow within a semi-circular cavity is simulated by the lattice Boltzmann method (LBM). The flow is evaluated for various Reynolds numbers, respectively. The treatment of curved boundary with secondary-order accurate is used. The numerical results show that when the Reynolds number is small, the final steady state consists of one vortex only. As the Reynolds number increases, a secondary vortex and then a tertiary vortex arises. In the case of a semi-circular cavity, the vortices develop at the bottom and as the Reynolds number increases, they grow pushing the main vortex to the right part of the cavity. Our results have a great agreement with [21] and further LBM has the capability to deal with the cases.

ACKNOWLEDGEMENTS

This work was supported by the 985 project of Jilin University (Grant No. 985). The authors would like to thank the reviewers of this article for their most helpful comments and suggestions.

REFERENCES

1. Qian YH, D'Humières D, Lallemand P. Lattice BGK models for Navier–Stokes equation. *Europhysics Letters* 1992; **17**:479–484.
2. Chen HD, Chen SY, Matthaeus WH. Recovery of the Navier–Stokes equations using a lattice-gas Boltzmann method. *Physical Review A* 1992; **45**:5339–5342.
3. Benzi R, Succi S, Vergassola M. The lattice Boltzmann equation: theory and applications. *Physics Reports* 1992; **222**:145–197.
4. Succi S, Yeomans JM. *The Lattice Boltzmann Equation for Fluid Dynamics and Beyond*. Oxford University Press: New York, 2001.

DOI: 10.1002/fld

5. Chen SY, Doolen GD. Lattice Boltzmann method for fluid flows. *Annual Review of Fluid Mechanics* 1998; **30**:329–364.
6. Qian YH, Succi S, Orszag SA. Recent advances in lattice Boltzmann computing. *Annual Review of Computational Physics* 1995; **3**:195–242.
7. Shi W, Hu S, Yan G. A lattice Boltzmann equation method for the shallow water wave equations. *ACTA Mechanica Sinica* 1997; **29**:525–529 (in Chinese).
8. Shi W, Shyy W, Mei R. Finite difference-based lattice-Boltzmann method for inviscid compressible flows. *Numerical Heat Transfer Part B* 2001; **40**:1–21.
9. Frisch U, Hasslacher B, Pomeau Y. Lattice-gas automata for the Navier–Stokes equation. *Physical Review Letters* 1986; **56**:1505–1508.
10. He X, Luo LS. A prior derivation of the lattice Boltzmann equation. *Physical Review E* 1997; **55**:R6333–R6336.
11. He X, Luo LS. Theory of the lattice Boltzmann method: from the Boltzmann equation to the lattice Boltzmann equation. *Physical Review E* 1997; **56**:R6811–R6817.
12. Yu D, Mei R, Luo LS, Shyy W. Viscous flow computations with the method of lattice Boltzmann equation. *Progress in Aerospace Sciences* 2003; **39**:329–367.
13. Hou S, Zou Q, Chen S, Doolen G, Cogley AC. Simulation of cavity flow by the lattice Boltzmann method. *Journal of Computational Physics* 1995; **118**:329–347.
14. Guo Z, Shi B, Wang N. Lattice BGK model for incompressible Navier–Stokes equation. *Journal of Computational Physics* 2000; **165**:288–306.
15. Chew YT, Shu C, Niu XD. A new differential lattice Boltzmann equation and its application to simulate incompressible flows on non-uniform grids. *Journal of Statistical Physics* 2002; **107**:329–342.
16. Ghia U, Ghia KN, Shin CT. High-Re solutions for incompressible flow using Navier–Stokes equations and a multigrid method. *Journal of Computational Physics* 1982; **48**:387–411.
17. Erturk E, Corke TC, Gökcöl C. Numerical solutions of 2-D steady incompressible driven cavity flow at high Reynolds numbers. *International Journal for Numerical Methods in Fluids* 2005; **48**:747–774.
18. Nishida H, Satofuka N. Higher-order solutions of square driven cavity flow using a variable-order multi-grid method. *International Journal for Numerical Methods in Fluids* 1992; **34**:637–653.
19. Belhachmi Z, Bernardi C, Karageorghis A. Spectral element discretization of the circular driven cavity. Part IV: the Navier–Stokes equations. *Journal of Mathematical Fluid Mechanics* 2004; **6**:121–156.
20. Glowinski R, Juárez LH. Finite element method and operator splitting for a time-dependent viscous incompressible free surface flow. *International Journal of Computational Fluid Dynamics* 2003; **12**:459–468.
21. Glowinski R, Guidoboni G, Pan T-W. Wall-driven incompressible viscous flow in a two-dimensional semi-circular cavity. *Journal of Computational Physics* 2006; **216**:76–91.
22. Pan T-W, Glowinski R. A projection/wave-like equation method for the numerical simulation of incompressible viscous fluid flow modeled by the Navier–Stokes equations. *International Journal of Computational Fluid Dynamics* 2000; **9**:28–42.
23. Auteri F, Parolini N, Quartapelle L. Numerical investigation on the stability of the singular driven cavity flow. *Journal of Computational Physics* 2002; **183**:1–25.
24. Migeon C, Texier A, Pineau G. Effects of lid-driven cavity shape on the flow establishment phase. *Journal of Fluids and Structures* 2000; **14**:469–488.
25. Bhatnagar PL, Gross EP, Krook M. A model for collision processes in gases. *Physical Review* 1954; **94**:511–525.
26. He X, Zou Q, Luo LS, Dembo M. Analytic solutions of simple flows and analysis of nonslip boundary conditions for the lattice Boltzmann BGK model. *Journal of Statistical Physics* 1997; **87**:115–136.
27. Mei R, Yu D, Shyy W, Luo L. Force evaluation in the lattice Boltzmann method involving curved geometry. *Physics Review E* 2002; **65**:041203/1–041203/14.
28. Filippova O, Hänel D. Grid refinement for lattice-BGK models. *Journal of Computational Physics* 1998; **147**: 219–228.
29. Mei R, Luo L, Shyy W. An accurate curved boundary treatment in the lattice Boltzmann method. *Journal of Computational Physics* 1999; **155**:307–330.

DOI: 10.1002/fld